Draft version February 2, 2008
Preprint typeset using LaTeX style emulateapj v. 6/22/04

THE NATURE OF LUMINOUS X-RAY SOURCES WITH MID-INFRARED COUNTERPARTS

A. Alonso-Herrero[1,2], P. G. Pérez-González[1], J. Rigby[1], G. H. Rieke[1], E. Le Floc'h[1], P. Barmby[3], M. J. Page[4], C. Papovich[1], H. Dole[5,1], E. Egami[1], J.-S. Huang[3], D. Rigopoulou[6], D. Cristóbal-Hornillos[7], C. Eliche-Moral[7], M. Balcells[7], M. Prieto[7], P. Erwin[7], C. W. Engelbracht[1], K. D. Gordon[1], M. Werner[8], S. P. Willner[3], G. G. Fazio[3], D. Frayer[9], D. Hines[1], D. Kelly[1], W. Latter[9], K. Misselt[1], S. Miyazaki[10], J. Morrison[1], M. J. Rieke[1], G. Wilson[9]

Draft version February 2, 2008

ABSTRACT

We investigate the luminous X-ray sources in the Lockman Hole (LH) and the Extended Groth Strip (EGS) detected at 24 μm using MIPS and also with IRAC on board *Spitzer*. We assemble optical/infrared spectral energy distributions (SEDs) for 45 X-ray/24 μm sources in the EGS and LH. Only about 1/4 of the hard X-ray/24μm sources show pure type 1 AGN SEDs. More than half of the X-ray/24 μm sources have stellar-emission-dominated or obscured SEDs, similar to those of local type 2 AGN and spiral/starburst galaxies. One-third of the sources detected in hard X-rays do not have a 24 μm counterpart. Two such sources in the LH have SEDs resembling those of S0/elliptical galaxies. The broad variety of SEDs in the optical-to-*Spitzer* bands of X-ray selected AGN means that AGN selected according to the behavior in the optical/infrared will have to be supplemented by other kinds of data (e.g., X-ray) to produce unbiased samples of AGN.

Subject headings: Infrared: galaxies — X-rays: galaxies — galaxies: active

1. INTRODUCTION

The very rapid evolution of quasars from $z \sim 2$ to the present (Boyle et al. 1987) raises the question of whether any properties of these sources other than space density have changed over this interval. One way to probe changes in the AGN population is to compare spectral energy distributions (SEDs) over a broad frequency range as a function of redshift. The SED of an active galaxy reflects the presence of the underlying AGN, plus the luminosity of the host galaxy stellar population, the reddening of the AGN, and the role of star formation, all in different frequency regimes. SED determination in large samples of high-z AGN using imaging detectors is therefore an efficient way to survey for evolutionary trends in quasars and AGN, and in their host galaxies.

A number of trends might be expected. Will we be able to confirm predictions that the relative number of obscured AGN was higher at large lookback times than now, to fit models of the X-ray background (e.g., Gilli, Risaliti, & Salvati 1999)? AGN activity may be triggered by gas inflow caused by galaxy interactions. Interactions also trigger starbursts — will we find that an elevated rate of star formation in the host galaxy is a typical characteristic of distant AGN? Will younger AGN host galaxies have more material in their ISM than current-epoch ones, causing greater extinction of their nuclei?

To probe such questions, we have used IRAC (Fazio et al. 2004), MIPS (Rieke et al. 2004), and ancillary data to assemble SEDs for AGN in the Lockman Hole (LH) and Extended Groth Strip (EGS). We have made use of deep X-ray images to locate the AGN. For this initial survey, we wanted an unambiguous detection of an infrared (IR) excess to make SED classification robust. We have included objects detected at 24 μm, although we briefly discuss galaxies not detected at 24 μm. We compare the results with SEDs of a sample of nearby ($z < 0.12$) hard X-ray selected AGN that are bright in the mid-IR, and hence nominally similar to the sources identified in the deep *Spitzer*/X-ray fields. This comparison allows us to make tentative identifications of trends in the AGN/host galaxy behavior from the typical redshift of the AGN in the survey fields ($z \sim 0.2$ to 1.6) to the present.

2. SPITZER OBSERVATIONS

We have obtained 24 μm MIPS observations of two fields in the LH: primary field (area of $5' \times 5'$) at RA = $10^{\rm h}\,52^{\rm m}$ and Dec = $57^\circ\,25'$ (J2000), and parallel field (area of $7' \times 6'$) at RA = $10^{\rm h}\,52^{\rm m}$ and Dec = $57^\circ\,37'$. We also obtained MIPS observations of the EGS overlapping with the *Chandra* observation ($\simeq 180\,{\rm arcmin}^2$, see next section) at RA = $14^{\rm h}\,17^{\rm m}$ and Dec = $52^\circ\,28'$. Gordon et al. (2004), Egami et al. (2004), Papovich et al. (2004), and Le Floc'h et al. (2004) describe the data reduction and photometry in detail. The astrometric uncertainties of *Spitzer* observations are $< 1''$. The 80% completeness limits at 24 μm are: 0.17 mJy and 0.1 mJy for the LH primary and parallel fields, and 0.11 mJy for the EGS (Papovich et al. 2004).

The LH primary field and the EGS were observed by IRAC at 3.6, 4.5, 5.8, and 8 μm. The data reduction is discussed in Huang et al. (2004) for the LH and Barmby et al. (2004, in preparation) for the EGS. Counterparts

[1] Steward Observatory, The University of Arizona, Tucson, AZ 85721; e-mail: aalonso@as.arizona.edu
[2] IEM, CSIC, E-28006 Madrid, Spain
[3] Harvard-Smithsonian Center for Astrophysics, Cambridge, MA 02138
[4] Mullard Space Science Laboratory, University College London, Dorking, Surrey, RH5 6NT, U. K.
[5] Institut d'Astrophysique Spatiale, bât 121, Université Paris Sud, F-91405 Orsay Cedex, France
[6] Department of Astrophysics, Oxford University, Keble Rd, Oxford, OX1 3RH, U. K.
[7] Instituto de Astrofísica de Canarias, E-38200 La Laguna, Spain
[8] Jet Propulsion Laboratory, Caltech, Pasadena, CA 91109
[9] Spitzer Science Center, Caltech, Pasadena, CA 91125
[10] Subaru Telescope, National Astronomical Observatory of Japan, Hilo, HI 96720

of all MIPS and X-ray sources were nearly pointlike, and the photometry used circular apertures and the standard point-source calibration (see Huang et al. 2004).

3. X-RAY OBSERVATIONS

The *XMM* images of the LH were formed from seven datasets taken in 2000 and 2001 to a total integration time of 150 ks. The data cover entirely both the primary and parallel 24 μm MIPS fields. We produced images in the energy bands $0.2-0.5$ keV, $0.5-2$ keV, $2-5$ keV, and $5-10$ keV, and searched for sources simultaneously in an iterative process to optimize the background model and thereby the sensitivity. In the LH we have detected 35 XMM sources with X-ray fluxes down to $f_{0.2-10\rm keV} \simeq 10^{-15}$ erg cm^{-2} s^{-1}. The astrometric uncertainties are better than $1''$ for bright sources, and less than $3''$ for the faintest sources.

For the EGS, three *Chandra* ACIS datasets were taken from the CXC archive with an exposure time of 131 ks. We searched for sources separately in four bands ($0.5-8$ keV, $0.5-2$ keV, $2-8$ keV, and $4-8$ keV) using WAVDETECT. In the overlapping area between the *Chandra* and MIPS fields we have detected 77 sources in the full band with fluxes down to $f_{0.5-8\rm keV} \simeq 10^{-15}$ erg cm^{-2} s^{-1}. Of these, 40 are detected in the $2-8$ keV band. Astrometric uncertainties are $1-2''$, where the high value is for sources at large off-axis angles.

4. CROSS-CORRELATION OF X-RAY AND 24 μM SOURCES

Taking into account the astrometric uncertainties we used radii of $2.2''$ and $3''$ for matching 24 μm sources to Chandra and XMM sources, respectively. Within the LH approximately 57% of the XMM sources are detected at 24 μm. 75% of LH X-ray sources with $f_{5-10\rm keV} > 10^{-15}$ erg cm^{-2} s^{-1} have 24 μm counterparts. In the EGS approximately 50% of Chandra sources have a 24 μm counterpart, and this fraction is $\simeq 60$% for sources detected in the hard ($2-8$ keV) band. Taking into account the surface density of 24 μm sources (80% completeness limit), the probability of a chance match with an X-ray source is $2-3$% for both the LH and EGS.

5. ACTIVITY CLASSIFICATION

Hard X-ray to mid-IR flux ratios are known to be different for AGN dominated galaxies and starbursts in the Local Universe, and can be used to assess if the AGN emission is dominant in the mid-IR. Fig. 1 shows the 24 μm fluxes vs. $2-10$ keV X-ray fluxes for our sample. As a comparison we plot the extrapolation to fainter fluxes of the region occupied by hard X-ray selected AGN from Piccinotti et al. (1982) with detected mid-IR emission and $z < 0.12$. This sample should be nominally similar to the sources studied here. The effect of increasing redshift on the observed ratio of hard X-ray to mid-IR fluxes is small for AGN with low X-ray column densities, but it will make this ratio increase for Compton thick AGN at higher z (Alexander et al. 2001). For starbursts at $z < 1$, Alexander et al. (2001) predict just a slight decrease of the ratio of hard X-ray to mid-IR emission for increasing z. The majority of sources in this study appear to derive their X-ray emission from powerful AGN because they lie in the region of Fig. 1 populated by local hard X-ray-selected AGN extrapolated to fainter fluxes (Fadda et al. 2002; Franceschini et al. 2001; Alexander et al. 2001), and because for our sample the z-dependent effects (see next section) in this figure are small.

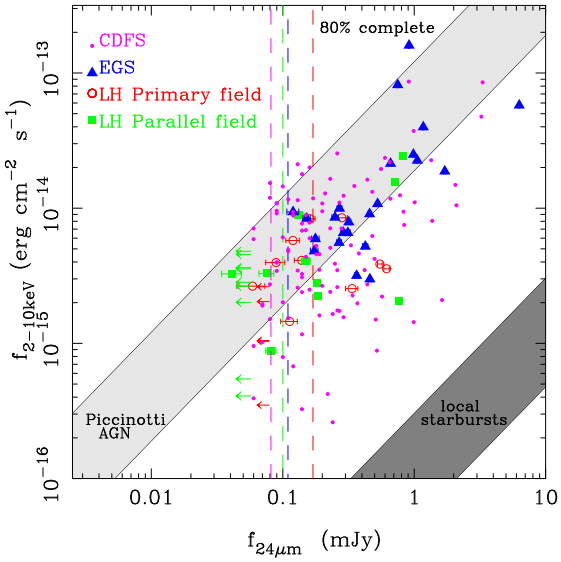

FIG. 1.— 24 μm fluxes vs. $2-10$ keV X-ray fluxes: XMM sources (squares and open circles) in the LH and Chandra sources in the EGS (filled triangles). The Chandra $2-8$ keV fluxes have been converted to $2-10$ keV assuming a power law with photon index $\Gamma = 1.4$. Also shown are X-ray/24 μm sources in the CDF-S (dots, Rigby et al. 2004). The 24 μm non-detections of LH X-ray sources are shown as upper limits at a 5σ confusion limit. The dashed lines are the 80% completeness limits for the different fields (color coded as the symbols for the different fields). The lightly shaded area is the extrapolation of the median hard X-ray to mid-IR ratios ($\pm1\sigma$) of local ($z < 0.12$) hard X-ray selected AGN (Piccinotti et al. 1982) with mid-IR emission. The dark shaded area is the extrapolation of local starburst galaxies from Ranalli, Comastri, & Setti (2003).

Also shown in Fig. 1 are sources in the Chandra Deep Field South (CDF-S) from Rigby et al. (2004). The greater sensitivity of the CDF-S X-ray data (compared with the EGS and LH) results in detection of relatively weaker X-ray sources that either have a greater portion of their luminosity generated from star formation, or are obscured in the X-rays (compare to figure 1 in Alexander et al. 2002). Indeed, spectroscopic observations of faint sources detected in the deepest X-ray surveys to date indicate that these are starbursts and low-redshift normal galaxies (Barger et al. 2003).

All X-ray sources in the LH not detected at 24 μm appear to be consistent with being type 1 AGN or S0/elliptical galaxies (see next section). Alexander et al. (2002) found that most X-ray emitting galaxies in the HDF-N with no mid-IR emission are classified spectroscopically as S0/elliptical galaxies; that is, they showed no emission-line evidence for activity.

X-ray hardness ratios can be used to distinguish between low-obscuration (soft) and high-obscuration (hard) AGN (e.g., Hasinger et al. 2001; Mainieri et al. 2002; Szokoly et al. 2004). This X-ray classification agrees with the spectroscopic classification of type 1 (broad lines) and type 2 (narrow lines) AGN, respectively. Based on their hard to soft flux ratios, there are approximately equal numbers of type 1 and type 2 AGN among the hard X-ray selected sources in the LH and EGS with and without mid-IR emission. This finding is in contrast with the local sample of hard X-ray selected AGN

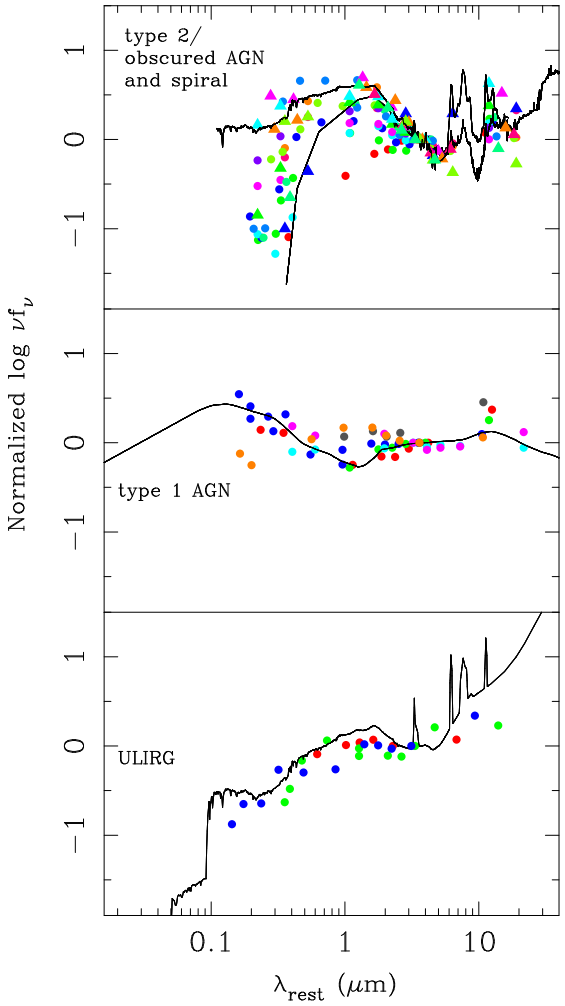

FIG. 2.— SED (normalized at $\lambda_{rest} \simeq 3.5\,\mu$m) types for EGS X-ray/24 μm sources (filled circles or triangles of different colors, for clarity; Table 1) with photometric redshifts estimated by us or redshifts from the literature. The ULIRGs SED class is shown with the Mkn 273 template from Devriendt et al. (1999); the type 1 AGN SED class is shown with the median QSO of Elvis et al. (1994). Obscured AGN/type 2 AGN/spiral SED galaxies are intermediate between the Circinus template (lower one) and the M82-like template (upper one) of Le Floc'h et al. (2004).

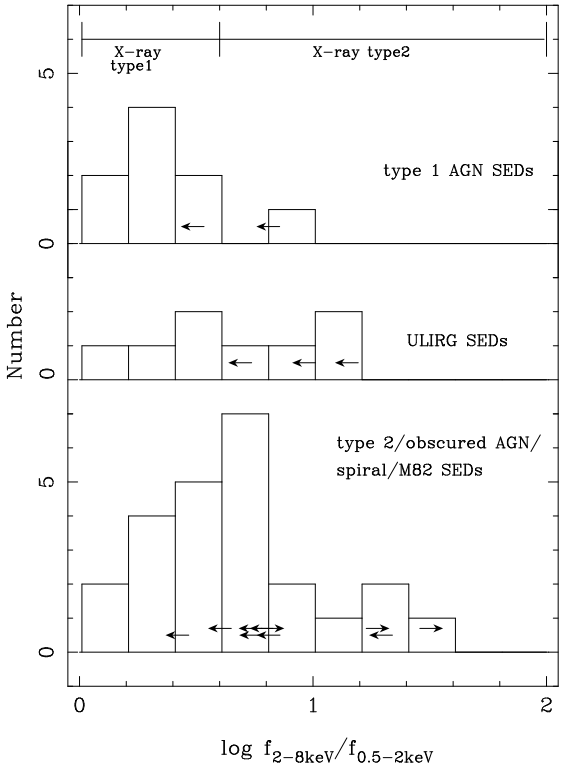

FIG. 3.— Hard to soft flux ratio distributions for the SED types (Fig. 2) of bright X-ray/24 μm sources in the LH and EGS. The approximate division between type 1 and type 2 AGN is also shown (Rigby et al. 2004 based on Szokoly et al. 2004). The arrows inside the histogram bins indicate sources with upper or lower limits to the hard to soft flux ratios.

of Piccinotti et al. (1982) where most of the sources are classified as type 1 AGN (70−80% for AGN at $z < 0.12$).

6. SPECTRAL ENERGY DISTRIBUTIONS

We have collected optical and near-IR data for all the X-ray/24μm sources in the EGS and LH (Cristóbal-Hornillos et al. 2003; Wilson 2003). The observations have been band merged with the *Spitzer* data as described by Le Floc'h et al. (2004) We used spectroscopic and photometric redshifts for 5 X-ray sources in the LH (Lehmann et al. 2001; Mainieri et al. 2002) and 9 sources in the EGS (from the Deep Extragalactic Evolutionary Probe and Miyaji et al. 2004). For the remaining sources, we estimated photometric redshifts where possible from the stellar spectral peak at $\lambda_{rest} = 1.6\,\mu$m (see Le Floc'h et al. 2004).

We then classified the X-ray/24 μm sources according to the shape of their SEDs. Sources that are relatively flat in νf_ν from the optical through the mid-IR, resembling the median QSO SED of Elvis et al. (1994), are termed type 1 AGN (Fig. 2). Sources that are relatively flat in νf_ν at the IRAC and MIPS wavelengths, but whose spectra drop toward the blue are consistent with being obscured AGN. Although the redshifts cannot be estimated well for these two types of objects, the SEDs are distinctive and the classification unambiguous. Galaxies with decreasing νf_ν in the range $\lambda_{obs} = 3.6 - 8\,\mu$m and a significant stellar contribution in the optical and near-IR resemble type 2 AGN or spiral/starburst galaxies, and their SEDs appear intermediate between that of Circinus and that of M82 (Fig. 2). The majority of these sources have spectroscopic/photometric redshifts in the range $z = 0.2 - 1.6$. A few galaxies have increasing νf_ν for $\lambda_{obs} \geq 3.6\,\mu$m, and look similar to local ULIRGs (Fig. 2). Table 1 lists the X-ray properties and SED types for those EGS sources with well determined SEDs (Fig. 2).

For the 45 X-ray/24μm sources in our sample with SED type, we find that 10 can be classified as pure type 1 AGN SED, 27 as obscured AGN, type 2 AGN, or spiral/M82-like SED, and 8 as ULIRG-like SED. In the absence of quality X-ray data, the optical-to-mid-IR SED does not unambiguously identify AGN activity. This will complicate efforts to identify complete samples of AGN via optical and *Spitzer* photometry.

Fig. 3 shows the hard to soft X-ray flux ratio distributions for the three different types of SEDs. All galaxies with type 1 AGN-like SEDs show a range of hard to soft flux ratios consistent with those of spectroscopically clas-

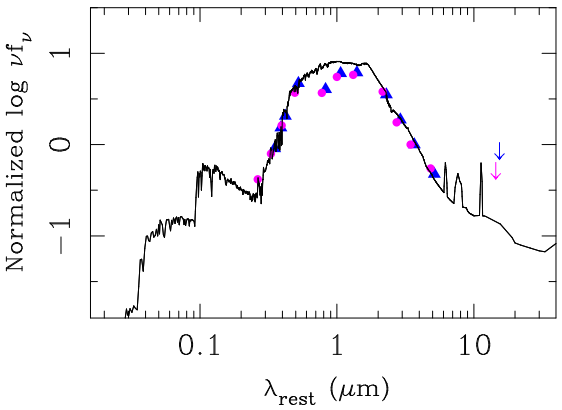

FIG. 4.— SEDs (normalized as in Fig. 2) of two LH sources — XMMJ105154.3+572753.2 (circles) and XMMJ105203.8+572339.3 (triangles) — not detected at 24 μm. Their SEDs are shown with an S0/Sa galaxy template from Devriendt et al. (1999).

sified type 1 AGN (that is, broad-line AGN). Galaxies with obscured AGN, type 2 AGN, and spiral/M82-like SEDs include a fraction of sources that would be classified as type 1 AGN based on their X-ray properties. ULIRG-SED objects appear to have a tendency toward softer X-ray flux ratios characteristic of type 1 AGN.

More than half of the bright X-ray/24 μm sources in our sample have SEDs dominated by stellar emission or show a significant level of obscuration. This is consistent with the finding that $40-60\%$ of the Chandra selected galaxies have optical spectra with no signs of nuclear AGN activity (e.g., Barger et al. 2001; Hornschemeier et al. 2001). Many of these galaxies have colors of old stellar populations (Barger et al. 2003). It is possible that their AGN emission lines are overwhelmed by stellar light (see Moran, Filippenko, & Chornock 2002). Others appear highly absorbed in X-rays (Barger et al. 2001, see also Fig. 3); if a similar level of absorption applies to their emission lines, these lines will be undetectable. In agreement with the finding that spectroscopic type 1 (broad lines) AGN behavior is relatively rare (e.g., Hornschemeier et al. 2001), the fraction of type 1 AGN SED dominated X-ray sources in our sample is small.

About one-third of the sources with emission in hard X-rays are not detected at 24 μm. Fig. 4 shows two such X-ray sources in the LH whose SEDs are consistent with being S0 or elliptical galaxies, with no evidence for the presence of hot dust. Based on findings by Alexander et al. (2002) for the HDF-N, a significant fraction of X-ray sources detected by IRAC but not by MIPS at 24 μm are likely to have SEDs like elliptical and S0 galaxies.

To put these trends on a more quantitative basis, we have used local hard-X-ray selected AGN from Piccinotti et al. (1982) and Kuraszkiewicz et al. (2003) to construct a comparison sample consisting of all galaxies with $z \leq 0.12$ and a mid-IR 25 μm flux density > 100 mJy. In this local sample, 19 of 32 galaxies, more than half the sample, would be classified by us as type 1 AGN based on their SEDs. From the hard X-ray/24 μm detections in the EGS and LH, we classify 7 of 29 as having SEDs resembling those of type 1 AGN. Since only 2/3 of sources with hard X-ray emission were detected at 24 μm, some caution is needed in interpreting this result. However, since a significant fraction of the X-ray sources without 24 μm detections are likely to have S0/elliptical type SEDs, it is possible that there is a trend away from pure type 1 AGN behavior with increasing redshift. This possibility will be probed by further *Spitzer* observations of deep X-ray fields that are currently under analysis.

This work is based [in part] on observations made with the Spitzer Space Telescope, which is operated by the Jet Propulsion Laboratory, Caltech under NASA contract 1407. Support for this work was provided by NASA through Contract no. 960785 issued by JPL/Caltech.

REFERENCES

Alexander, D. M. et al. 2001, ApJ, 554, 18
Alexander, D. M. et al. 2002, ApJ, 568, L85
Barger, A. J. et al. 2003, AJ, 126, 632
Barger, A. J. et al. 2001, AJ, 121, 662
Boyle, B. J. et al. 1987, MNRAS, 227, 717
Cristóbal-Hornillos et al. 2003, ApJ, 595, 71
Devriendt, J. E. G. et al. 1999, A&A, 350, 381
Egami, E. et al. 2004, in this volume
Elvis, M. et al. 1994, ApJS, 95, 1
Fadda, D. et al. 2002, A&A, 383, 838
Fazio, G. G. et al. 2004, this volume
Franceschini, A. et al. 2002, ApJ, 568, 470
Gilli, R., Risaliti, G., & Salvati, M. 1999, A&A, 347, 424
Gordon, K. et al. 2004, PASP, submitted
Hasinger, G. et al. 2001, A&A, 365, L50
Hornschemeier, A. E. et al. 2001, ApJ, 554, 742
Huang, J.-S. et al. 2004, this volume
Kuraszkiewicz, J. K. et al. 2003, ApJ, 590, 128
Le Floc'h, E. et al. 2004, this volume
Lehmann, I. et al. 2001, A&A, 371, 833
Mainieri, V. et al. 2002, A&A, 393, 42
Miyaji, T. et al. 2004, AJ, in press (astro-ph/0402617)
Moran, E. C. et al. 2002, ApJ, 579, 71
Papovich, C. et al. 2004, this volume
Piccinotti, G. et al. 1982, ApJ, 253, 485
Ranalli, P., Comastri, A., & Setti, G. 2003, A&A, 399, 39
Rieke, G. H. et al. 2004, this volume
Rigby, J. et al. 2004, this volume
Szokoly, G. P. et al. 2004, ApJS, astro-ph/0312324
Wilson, G. 2003, ApJ, 585, 191

TABLE 1
Chandra positions and fluxes, and SED types for X-ray galaxies in the EGS with well determined SED types.

RA	DEC	d	f(0.5-8keV)	error	d	f(0.5-2keV)	error	d	f(2-8keV)	error	SED type
(1)	(2)	(3)	(4)	(5)	(6)	(7)	(8)	(9)	(10)	(11)	(12)
214.189607	52.485142	1	0.244E-13	0.237E-14	1	0.425E-14	0.514E-15	0	0.232E-13	–	ULIRG
214.333361	52.416680	1	0.573E-14	0.114E-14	1	0.713E-15	0.219E-15	1	0.471E-14	0.146E-14	ULIRG
214.486947	52.523481	1	0.809E-14	0.129E-14	1	0.131E-14	0.296E-15	1	0.522E-14	0.162E-14	ULIRG
214.355623	52.595469	1	0.535E-14	0.133E-14	1	0.107E-14	0.287E-15	0	0.770E-14	–	type 1 AGN
214.222970	52.352189	1	0.196E-13	0.299E-14	0	0.565E-14	–	0	0.225E-13	–	type 1 AGN
214.312620	52.387032	1	0.177E-13	0.197E-14	1	0.357E-14	0.472E-15	1	0.791E-14	0.192E-14	type 1 AGN
214.205410	52.425120	1	0.130E-12	0.593E-14	1	0.258E-13	0.140E-14	1	0.648E-13	0.576E-14	type 1 AGN
214.399811	52.508273	1	0.274E-12	0.640E-14	1	0.506E-13	0.149E-14	1	0.127E-12	0.554E-14	type 1 AGN
214.401378	52.595777	1	0.657E-14	0.140E-14	1	0.159E-14	0.342E-15	0	0.543E-14	–	type 1 AGN
214.395215	52.469626	1	0.342E-13	0.293E-14	1	0.615E-14	0.671E-15	1	0.170E-13	0.286E-14	type 1 AGN
214.424483	52.473194	1	0.807E-13	0.356E-14	1	0.141E-13	0.880E-15	1	0.458E-13	0.347E-14	type 2, obscured AGN, Spiral
214.441532	52.509038	1	0.243E-13	0.203E-14	1	0.315E-14	0.416E-15	1	0.179E-13	0.230E-14	type 2, obscured AGN, Spiral
214.439370	52.497597	1	0.572E-14	0.108E-14	1	0.233E-15	0.128E-15	1	0.856E-14	0.165E-14	type 2, obscured AGN, Spiral
214.348256	52.432237	1	0.175E-14	0.665E-15	0	0.421E-15	–	1	0.252E-14	0.116E-14	type 2, obscured AGN, Spiral
214.352513	52.506880	1	0.591E-13	0.310E-14	1	0.111E-13	0.736E-15	1	0.316E-13	0.292E-14	type 2, obscured AGN, Spiral
214.347510	52.531594	1	0.245E-13	0.217E-14	1	0.582E-14	0.576E-15	1	0.720E-14	0.175E-14	type 2, obscured AGN, Spiral
214.267749	52.414954	1	0.132E-13	0.168E-14	0	0.691E-15	–	1	0.198E-13	0.263E-14	type 2, obscured AGN, Spiral
214.253100	52.322161	1	0.463E-13	0.346E-14	0	0.137E-13	–	0	0.212E-13	–	type 2, obscured AGN, Spiral
214.213653	52.346056	1	0.457E-13	0.397E-14	1	0.871E-14	0.854E-15	0	0.389E-13	–	type 2, obscured AGN, Spiral
214.267911	52.361115	1	0.856E-14	0.173E-14	0	0.142E-14	–	0	0.181E-13	–	type 2, obscured AGN, Spiral
214.294179	52.474719	1	0.145E-13	0.179E-14	1	0.320E-14	0.444E-15	1	0.522E-14	0.172E-14	type 2, obscured AGN, Spiral
214.217017	52.450224	1	0.560E-14	0.144E-14	1	0.971E-15	0.290E-15	1	0.442E-14	0.184E-14	type 2, obscured AGN, Spiral
214.439939	52.460638	0	0.246E-14	–	1	0.101E-14	0.136E-15	0	0.221E-14	–	type 2, obscured AGN, Spiral
214.351131	52.541650	0	0.374E-14	–	1	0.380E-14	0.186E-15	0	0.231E-14	–	type 2, obscured AGN, Spiral
214.345872	52.528797	1	0.589E-14	0.117E-14	1	0.126E-14	0.330E-15	1	0.237E-14	0.126E-14	type 2, obscured AGN, Spiral
214.299767	52.336922	1	0.124E-12	0.488E-14	1	0.243E-13	0.114E-14	0	0.714E-13	–	type 2, obscured AGN, Spiral
214.313384	52.447367	1	0.650E-14	0.125E-14	1	0.622E-15	0.223E-15	1	0.679E-14	0.169E-14	type 2, obscured AGN, Spiral
214.203452	52.433096	1	0.106E-13	0.224E-14	1	0.187E-14	0.458E-15	0	0.135E-13	–	type 2, obscured AGN, Spiral
214.390994	52.563506	1	0.778E-14	0.130E-14	1	0.111E-14	0.273E-15	1	0.667E-14	0.160E-14	type 2, obscured AGN, Spiral

[This table will be published in the electronic edition of the Journal. The printed edition will contain only a sample.]
NOTES — In this table we list those EGS galaxies with well determined SED types and with an estimate of the redshift, that is, galaxies plotted in Fig. 2. Column (1): Chandra RA (J2000). Column (2): Chandra DEC (J2000). Column (3): detection in the full $(0.5-8\mathrm{keV})$ band (1=dectection, 0=3σ upper limit). Column (4): flux in the full $(0.5-8\mathrm{keV})$ band in erg cm^{-2} s^{-1}. Column (5): error of flux in the full $(0.5-0.8\mathrm{keV})$ band in erg cm^{-2} s^{-1}. Column (6): detection in the soft $(0.5-2\mathrm{keV})$ band (1=dectection, 0=3σ upper limit). Column (7): flux in the soft $(0.5-2\mathrm{keV})$ band in erg cm^{-2} s^{-1}. Column (8): error of flux in the soft $(0.5-2\mathrm{keV})$ band in erg cm^{-2} s^{-1}. Column (9): detection in the hard $(2-8\mathrm{keV})$ band (1=dectection, 0=3σ upper limit). Column (10): flux in the hard $(2-8\mathrm{keV})$ band in erg cm^{-2} s^{-1}. Column (11): error of flux in the hard $(2-8\mathrm{keV})$ band in erg cm^{-2} s^{-1}. Column (12): SED type (see Fig. 2, and text).